Construction of a 4D Brain Atlas and Growth Model Using Diffeomorphic Registration

Andreas Schuh[1](✉), Maria Murgasova[2], Antonios Makropoulos[1], Christian Ledig[1], Serena J. Counsell[2], Jo V. Hajnal[2], Paul Aljabar[2], and Daniel Rueckert[1]

[1] Imperial College London, London, UK
a.schuh12@imperial.ac.uk
[2] King's College London, London, UK

Abstract. Atlases of the human brain have numerous applications in neurological imaging such as the analysis of brain growth. Publicly available atlases of the developing brain have previously been constructed using the arithmetic mean of free-form deformations which were obtained by asymmetric pairwise registration of brain images. Most of these atlases represent cross-sections of the growth process only. In this work, we use the Log-Euclidean mean of inverse consistent transformations which belong to the one-parameter subgroup of diffeomorphisms, as it more naturally represents average morphology. During the registration, similarity is evaluated symmetrically for the images to be aligned. As both images are equally affected by the deformation and interpolation, asymmetric bias is reduced. We further propose to represent longitudinal change by exploiting the numerous transformations computed during the atlas construction in order to derive a deformation model of mean growth. Based on brain images of 118 neonates, we constructed an atlas which describes the dynamics of early development through mean images at weekly intervals and a continuous spatio-temporal deformation. The evolution of brain volumes calculated on preterm neonates is in agreement with recently published findings based on measures of cortical folding of fetuses at the equivalent age range.

1 Introduction

Brain atlases have numerous applications in neurological image analysis. Brain templates and tissue probability maps are frequently used for image segmentation [9,10]. Deformations encoding the average brain growth of a population may be analyzed to study brain development [1]. Only recently, spatio-temporal (4D) atlases of the developing human brain have become available: Habas et al. [7] created an atlas from 20 fetal Magnetic Resonance (MR) images from polynomial fits for parameters which describe global scaling, local deformations, and intensity changes. In contrast, Kuklisova-Murgasova et al. [9] used a non-parametric kernel regression of affine transformations to build an atlas of the preterm brain. This has been shown to improve intensity-driven tissue segmentation [9,10]. For

S. Durrleman et al. (Eds.): STIA 2014, LNCS 8682, pp. 27–37, 2015.
DOI: 10.1007/978-3-319-14905-9_3

other applications, such as structural segmentation and morphometry studies, templates with a greater level of anatomical detail are typically required.

A spatio-temporal atlas of high level of detail was created by Serag et al. [18] using pairwise free-form deformations (FFDs) [17] and kernel regression with time as dependent variable. The individual brain images are therefore mapped into the atlas space using the inverses of time-dependent average transformations which were computed in [18] based on the arithmetic mean of pairwise FFDs. This limits the atlas construction to small deformations between images as otherwise invertibility is not guaranteed.

A natural choice of average to represent mean morphology is given by the exponential map of the arithmetic mean of stationary velocity fields. The velocity fields are the generating elements of the Lie algebra [2] corresponding to the one-parameter subgroup of diffeomorphisms. We therefore propose an alternative approach to [18] based on a FFD model parameterized by a stationary velocity field that generates transformations with guaranteed invertibility. Our atlas construction is related to the kernel based shape regression proposed by Davis et al. [6] in that we also use a kernel method to regress a spatio-temporal template from cross-sectional images and use a diffeomorphic registration. Davis et al. utilize a groupwise template estimation [8] that minimizes a single objective function to find both the template image and the transformations which relate the individual to this mean image based on the sum of squared differences (SSD). In contrast, we first obtain the transformations which map each anatomy into a common atlas space and then compute the template image. This allows us to use different (dis-)similarity measures for the decoupled optimization problems. In particular, to deal with the wide MR intensity variations associated with myelination and other processes during early brain development, we compute all pairwise inter-subject transformations using an efficient diffeomorphic registration based on normalized mutual information (NMI). Given the one-to-one correspondences between the anatomies of different subjects of similar ages, we then estimate a mean image. We estimate the mean image such that it minimizes the SSD of the observations in the coordinate system, which requires the least residual deformation to explain the anatomical variability across all individuals.

Previous neonatal atlas construction methods [9,18] focused on the creation of age-specific mean brain templates with corresponding tissue probability maps. While these methods allow the generation of mean images at high temporal resolution, the resulting atlas only consists of cross-sections of the growth process. A deformable transformation model, which encodes the longitudinal changes that occur during a given time interval, would enable the analysis of the biological processes that underlie these changes based on the deformations.

Lately, generative models for the study of time series data and spatio-temporal atlas building based on an extension of the large deformation diffeomorphic metric mapping (LDDMM) registration have been proposed [15,19]. These models parameterize a time series of generally adult brain images by an initial image and initial momentum. Due to the significant age-related intensity variations, the time series of neonatal mean brain images cannot be represented by a single deformed mean image. Instead, we propose to represent longitudinal change by exploiting the numerous transformations between subjects of similar ages, computed during the construction of the atlas. The proposed method allows the derivation of a mean growth model from these transformations, without additional intensity-driven registration of the spatio-temporal atlas time points.

We provide qualitative evidence that the constructed atlas is of higher anatomical detail than other state-of-the-art neonatal brain atlases and that our growth model allows the accurate modeling of brain growth during early development.

2 Methods

2.1 Parametric Diffeomorphic Registration

The proposed spatio-temporal atlas construction method is based on pairwise image registration as schematically illustrated in Fig. 1a. The brain MR images are rigidly preregistered to a common image space. Registrations between all pairs of images (I_i, I_j) are then carried out in two stages. First, an affine registration is performed, followed by an inverse consistent registration which finds the spline coefficients of a stationary velocity field $\mathbf{v}_{ij}$ that minimizes the objective function. To avoid extrapolation of the initial global transformation outside the finite control point lattice, we model the transformation $\mathbf{T}_{ij}$ between an image pair as the sum of global and local velocity fields

$$\mathbf{T}_{ij} = \exp\left(\mathbf{v}_{ij}\right) = \exp\left(\mathbf{v}_{ij}^{global} + \mathbf{v}_{ij}^{local}\right) \tag{1}$$

where $\mathbf{v}_{ij}^{global} = \log\left(\mathbf{A}_{ij}\right)$. The logarithm of the 4x4 homogeneous coordinate transformation matrix, $\mathbf{A}_{ij}$, obtained by the initial affine registration, is computed using a Padé approximation [5]. The velocity field $\mathbf{v}_{ij}^{local}$ represents the local deformation to be optimized in the second stage and is given by

$$\mathbf{v}_{ij}^{local}\left(\mathbf{x}\right) = \sum_{c=1}^{m} \beta\left(\frac{x - x_c}{\delta x}\right) \beta\left(\frac{y - y_c}{\delta y}\right) \beta\left(\frac{z - z_c}{\delta z}\right) \boldsymbol{\nu}_{ij}^{(c)} \tag{2}$$

The m control points are defined on a regular lattice with spacing $(\delta x, \delta y, \delta z)^T$, where $\mathbf{x} = (x, y, z)^T$ and $(x_c, y_c, z_c)^T$ is the position of the c-th control point with spline coefficient vector $\boldsymbol{\nu}_{ij}^{(c)}$, and $\beta(\cdot)$ denotes the cubic B-spline function [17]. The use of a FFD model reduces the number of parameters of the stationary velocity field to be optimized and allows the analytic derivation.

In order to remove bias due to the direction of registration, which can be substantial as shown for hippocampal volume measurements in [22], and to obtain consistent pairwise transformations, we use a symmetric energy formulation. Using normalized mutual information (NMI) as similarity measure, the energy minimized by our registration with respect to the spline coefficients of the local velocity field component of $\mathbf{v}_{ij}$ is given by

$$E = -\lambda_1 \,\mathrm{NMI}\left(I_i \circ \mathbf{T}_{ij}^{-0.5}, I_j \circ \mathbf{T}_{ij}^{+0.5}\right) + \lambda_2 \,\mathrm{BE}\left(\mathbf{v}_{ij}\right) + \lambda_3 \,\mathrm{JAC}\left(\mathbf{v}_{ij}\right) \tag{3}$$

where

$$\mathbf{T}_{ij}^{\tau} = \exp\left(\tau \mathbf{v}_{ij}\right) \tag{4}$$

The non-negative constants $\lambda_{1,2,3}$ weigh the contribution of each term. Bending energy, BE, and a Jacobian-based penalty term, JAC, are used to prevent folding and tearing, i.e.,

$$\mathrm{BE}\left(\mathbf{v}\right) = \frac{1}{|\Omega|} \sum_{\mathbf{x}\in\Omega} \sum_{m=1}^{3} \sum_{n=1}^{3} \left(\frac{\partial^2 \mathbf{v}(\mathbf{x})}{\partial x_m \partial x_n} \right)^2 \tag{5}$$

$$\mathrm{JAC}\left(\mathbf{v}\right) = \frac{1}{|\Omega|} \sum_{\mathbf{x}\in\Omega} \log^2 \left(\det\left(\mathbf{J}_{\mathbf{v}}\left(\mathbf{x}\right)\right)\right) \tag{6}$$

where Ω denotes the finite set of positions on the transformed image lattice at which the energy is evaluated, and $\mathbf{J}_{\mathbf{v}}\left(\mathbf{x}\right)$ denotes the Jacobian matrix of the velocity field $\mathbf{v}$ evaluated at $\mathbf{x}$. This is similar to the approach of Modat et al. [13], as the exponential map is only guaranteed to generate a diffeomorphism when the velocity field is sufficiently smooth.

Our formulation differs from others by the use of a single parametric transformation and only one similarity evaluation as opposed to separate forward and backward transformations [3,12] or similarity evaluated twice [20]. The method is similar to that of [11] in that we transform both images half-way and use a single similarity term. The image similarity is therefore evaluated for images which are equally affected by the deformation and interpolation. Additionally, inverse consistency reduces the number of required pairwise registrations.

We use an approximate but fast scaling-and-squaring on the control point lattice as presented in [13] for the computation of the exponential map (4). Given the derivative of (3) with respect to $\boldsymbol{\nu}_{ij}$, we perform a conjugate gradient descent to find the set of parameters which minimize E.

The NMI gradient is first computed separately for each half transformation as in [14]. The resulting gradient fields are then added up with their corresponding weights $\tau = \pm 0.5$ to obtain the gradient field, $\delta \mathbf{u}_{ij}$. Note that the scaling factor τ accounts for both the averaging of the separate NMI gradient fields as well as the inversion of the gradient corresponding to the half backward transformation. The obtained gradient field is then composed with the current velocity field. This composition is approximated in the *log-domain* using the Baker-Campbell-Hausdorff (BCH) formula [20], i.e.,

$$\delta \mathbf{v}_{ij} = \delta \mathbf{u}_{ij} + \frac{1}{2}\left[\mathbf{v}_{ij}, \delta \mathbf{u}_{ij}\right] + \frac{1}{12}\left[\mathbf{v}_{ij}, \left[\mathbf{v}_{ij}, \delta \mathbf{u}_{ij}\right]\right] \tag{7}$$

where the first term of the BCH formula is omitted in order to obtain the difference between the two velocity field estimates. This computation is similar to the update step of the symmetric LogDemons [20]. By interpolating all vector fields (incl. the Lie bracket $[\cdot, \cdot]$) by cubic B-spline functions with control points defined on the same lattice as the local velocity field (2), the NMI gradient with respect to $\boldsymbol{\nu}_{ij}$ is approximated by the spline coefficients of (7).

The computation of the analytic gradient of the bending energy and the Jacobian-based penalty is identical to the classical FFD. The derivatives of these terms are given in [13,14].

2.2 Spatio-Temporal Atlas Construction

To avoid bias of the atlas towards a given anatomical configuration, we create the spatio-temporal atlas using pairwise inter-subject transformations. All pairwise transformations are hereby computed using the symmetric and inverse consistent diffeomorphic registration presented in the previous section. The anatomy of each subject is mapped by the inverse of the age-dependent Log-Euclidean mean [2] of the transformations relating it to the other subject anatomies of similar ages. This average transformation minimizes the weighted sum of squared distances to the observed inter-subject transformations, given the squared distance between two diffeomorphisms generated by stationary velocity fields as defined in [2], i.e.,

$$d^2(\mathbf{T}_1, \mathbf{T}_2) = \| \log(\mathbf{T}_1) - \log(\mathbf{T}_2)\|^2 \tag{8}$$

In particular, given n transformations $\mathbf{T}_{ij}$, which map an anatomical reference point $\mathbf{x}_i$ of subject i to their corresponding points $\mathbf{x}_j = \mathbf{T}_{ij}(\mathbf{x}_i)$ of subjects $j \in [1, n]$ (incl. the identity for $j = i$), the average transformation which maps $\mathbf{x}_i$ to its atlas coordinate at age t is given by

$$\bar{\mathbf{T}}_i\,(t) = \exp\left(\bar{\mathbf{v}}_i(t)\right) \tag{9}$$

where

$$\bar{\mathbf{v}}_i(t) = \frac{\sum_{j=1}^{n} w(t_j, t)\mathbf{v}_{ij}}{\sum_{j=1}^{n} w(t_j, t)} \tag{10}$$

with Gaussian kernel weights for the temporal regression, i.e.,

$$w(t_j, t) = \frac{1}{\sigma\sqrt{2\pi}} e^{\frac{-(t_j - t)^2}{2\sigma^2}} \tag{11}$$

The atlas template of mean shape and mean intensities at age t is then estimated as the image which minimizes the weighted sum of squared differences to the observations close to t, after mapping these into the respective atlas coordinate system, i.e.,

$$\bar{I}(t) = \frac{\sum_{i=1}^{n} w(t_i, t)\ I_i \circ \bar{\mathbf{T}}_i^{-1}(t)}{\sum_{i=1}^{n} w(t_i, t)} \tag{12}$$

Possibly available hard segmentation labels or probability maps can be transferred into the atlas space as well, using the computed inverse average transformations. Propagated hard segmentation masks are averaged using the same weights as in (12) to obtain separate mean probability maps for each class.

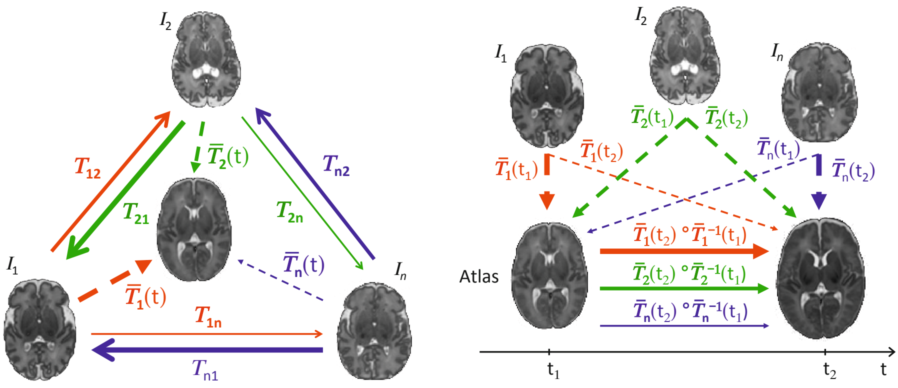

(a) cross-sectional (b) longitudinal

Fig. 1. Cross-sectional and longitudinal perspective on transformations computed during the atlas construction. The transformations $\bar{\mathbf{T}}_i(t)$ (dashed arrows) correspond to the Log-Euclidean mean of pairwise transformations $\mathbf{T}_{ij} = \mathbf{T}_{ji}^{-1}$ (solid arrows in a). The composite transformations shown in (b) are used to derive a longitudinal growth model. The non-uniform arrow weights depict the temporal kernel regression weights $w(t_j, t)$.

2.3 Atlas Growth Modeling

Examining the atlas construction as depicted in Fig. 1b, it can be seen that the anatomical point $\mathbf{x}_i$ of subject i is mapped by $\bar{\mathbf{T}}_i(t_1)$ to the atlas coordinate $(\mathbf{x}_1, t_1)$, and to $(\mathbf{x}_2, t_2)$ by the transformation $\bar{\mathbf{T}}_i(t_2)$. We therefore define a separate spatial mapping between two atlas time points for each subject. This is expressed in terms of the transformations that relate each time point to the individual as

$$\mathbf{G}_i(t_1, t_2) = \bar{\mathbf{T}}_i(t_2) \circ \bar{\mathbf{T}}_i^{-1}(t_1) \tag{13}$$

Noting that the transformations are generated by stationary velocity fields $\bar{\mathbf{v}}_i(t)$, we utilize the BCH formula [4] once more to approximate the stationary velocity field $\mathbf{g}_i(t_1, t_2)$ which generates the diffeomorphism $\mathbf{G}_i(t_1, t_2)$, i.e.,

$$\mathbf{g}_i(t_1, t_2) \approx \bar{\mathbf{v}}_i(t_2) - \bar{\mathbf{v}}_i(t_1) \tag{14}$$

More terms of the BCH formula may be used for a higher approximation order.

The longitudinal velocities $\mathbf{g}_i$ at the spatio-temporal atlas coordinates generate the diffeomorphic maps between corresponding points $\mathbf{x}_1$ and $\mathbf{x}_2$ for the time interval $[t_1, t_2]$ in accordance with the previously constructed time series of template images. We thus obtain the mean deformation between consecutive atlas time points using the same weights as in (12), i.e.,

$$\mathbf{G}(t_1, t_2) = \exp\left(\frac{\sum_{i=1}^{n} w(t_i, t_1)\mathbf{g}_i(t_1, t_2)}{\sum_{i=1}^{n} w(t_i, t_1)}\right) = \exp\left(\mathbf{g}(t_1, t_2)\right) \tag{15}$$

It should now be observed that the yet stationary velocity fields $\mathbf{g}(t_k, t_{k+1})$, which generate the diffeomorphic maps between consecutive time points, can be interpolated also in the time domain. The resulting time-varying spatio-temporal velocity field is continuous and therefore denoted here by $\tilde{\mathbf{g}}(\mathbf{x}, t)$. This deformation model enables the computation of point trajectories

$$\mathbf{x}(t_2) = \mathbf{x}_1 + \int_{t_1}^{t_2} \tilde{\mathbf{g}}(\mathbf{x}(t), t)dt \tag{16}$$

for any given initial atlas coordinate $(\mathbf{x}_1, t_1)$. The error arising from the concatenation and temporal interpolation of piecewise-stationary velocity fields decreases with increasing temporal resolution of the previously constructed atlas.

3 Results

3.1 Subjects

We used T2-weighted (T2-w) fast-spin echo images of 118 neonates acquired on a 3T Philips Intera system with MR sequence parameters TR=1712 ms, TE=160 ms, flip angle 90° and voxel size $0.86 \times 0.86 \times 1\,\text{mm}^3$. These images were randomly selected from 445 subjects, with at most 10 subjects from each week gestational age (GA) to reduce the number of pairs to register. This selection resulted in a close to uniform age at scan distribution. The age range at time of scan was 27.14 to 49.86 weeks GA, with mean and standard deviation of 36.40±5.70 weeks GA. The average age at birth was 29.14±3.22, range 24.29-39.71 weeks GA. Out of 118 subjects, 66 were female, and 52 male.

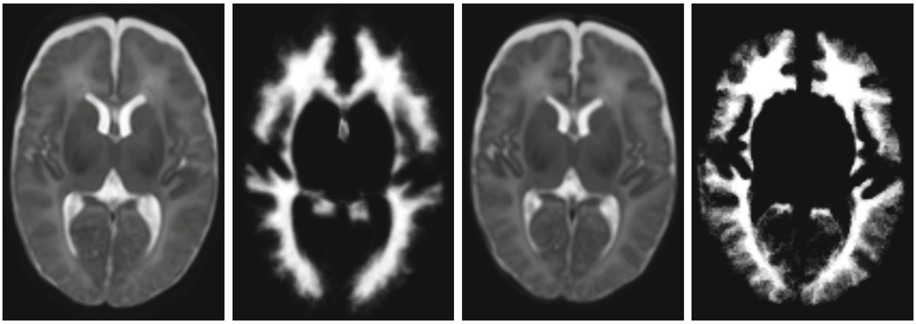

(a) (b) (c) (d)

Fig. 2. Comparison of T2-w templates and white matter maps at 42 weeks GA. The images were created in [18] using the arithmetic mean of FFDs (a)(b) and by our method using the Log-Euclidean mean of diffeomorphisms (c)(d).

3.2 Neonatal Brain Atlas

From the randomly selected subset of neonatal brain MR images, we constructed an atlas consisting of a time series of mean T2-w template images and corresponding tissue probability maps for the age range 28–44 weeks GA at regular time points for each week. Exemplary axial slices of these mean images are shown in Fig. 3 for qualitative assessment.

A comparison of the T2-w atlas template at age 42 weeks GA to the one created by Serag et al. [18], based on the arithmetic mean of FFDs, is given by Fig. 2. Our method notably captures the cortical folds of the frontal lobe with more detail, even though more images contributed to the average. As noted in [18], Serag et al. use on average 15–19 images per time point for the atlas construction, whereas given our dataset and a kernel width $\sigma = 0.5$ weeks, the proposed approach uses 19–28 images per time point, where images with kernel weight below 1% are not considered for the average. It should be noted that we used a constant kernel width because of the close to uniform age distribution of our randomly selected subjects, in which case also the subdivision algorithm used in [18] would result in a nearly constant kernel width. An adaptive kernel width may be used in case of a non-uniform sample distribution. It should also be noted, that the atlas created by Serag et al. was created from a different subset of available neonatal brain images than the atlas presented in Fig. 3.

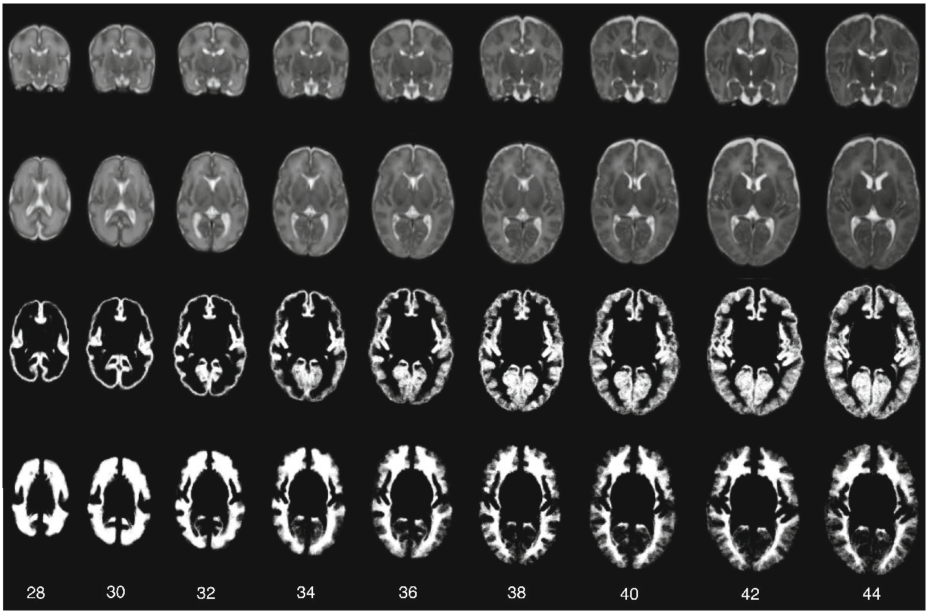

Fig. 3. T2-w templates, cortical grey matter, and white matter maps of our atlas

3.3 Brain Growth Model

We estimated the longitudinal velocities, $\mathbf{g}(t_k, t_{k+1})$, from the subject- and age-dependent average velocity fields which were also used to compute the time series of mean template images of the atlas. These stationary velocity fields were interpolated in both space and time by a cubic B-spline in order to obtain a continuous spatio-temporal growth model. We then used this deformation model to transform the mean tissue probability maps of the atlas at 44 weeks GA backward in time using the computed longitudinal point trajectories. As the longitudinal growth model is diffeomorphic, the probability maps from 28 weeks GA (or any other time point) could also be propagated forward (and backward) in time, which would result in very similar deformed tissue maps because the point trajectories given by (16) only differ by a small error resulting from the numerical integration. The decision to propagate the probability maps backwards in time has the advantage of a lower interpolation error close to anatomical boundaries due to the higher detail and bigger scale of the anatomy at later time points. From the propagated probability maps, we extracted the total volume of brain tissue and the cortical grey matter volume at one week intervals. The measured volumes, plotted against age at scan in Fig. 4, exhibit a Gompertz like growth pattern with a high R^2 value of 0.996 in both cases. This finding is in agreement with the results in [21], where cortical folding of fetuses was measured instead of cortical grey matter volume of preterm born neonates. While a cubic polynomial yielded a similar good fit for our measured brain volumes, we chose the Gompertz function because it has better extrapolation properties and was demonstrated to model the evolution of cortical folding during early brain development better than linear or quadratic polynomial functions [21].

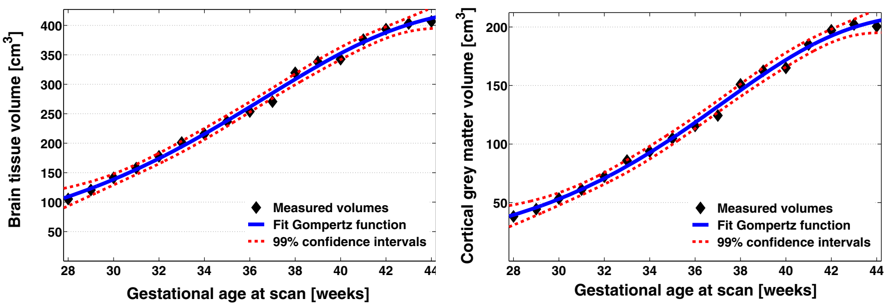

Fig. 4. Mean volumes of brain tissue and cortical grey matter plotted against age at time of scan. The volumes were extracted from the mean tissue probability maps at age 44 weeks GA, after propagating these backward in time using our continuous longitudinal growth model. A Gompertz function (solid line) was fitted to the data points and 99% confidence intervals (dashed lines) are shown.

4 Conclusions

We presented a method for the construction of a spatio-temporal atlas of high anatomical detail based on the Log-Euclidean mean of transformations which belong to the one-parameter subgroup of diffeomorphisms. We also utilized the numerous pairwise inter-subject transformations used to construct the atlas time series to derive a longitudinal deformation model of mean growth. This avoids additional intensity-driven registration of the atlas time points. A longitudinal registration of the template images has to account for the MR intensity changes which are associated with the ongoing myelination and other processes during early brain development such that these are not reflected in the deformation. By opportunely combining the cross-sectional transformations which map the individual to each atlas time point, we obtain a mean growth model directly from the inter-subject registrations. While the atlas itself captures brain growth only at discrete time points, our continuous growth model allows the analysis of growth trajectories between any two time points of the captured age range.

Compared to the first months after birth, the MR intensity changes are relatively moderate within the neonatal age range that we focused on in this work. The NMI similarity measure used for the pairwise registrations is, however, a well-established image similarity measure in inter-subject and multi-modality image registration [16]. It has demonstrated to be robust to wide intensity variations and could thus be employed for the construction of a spatio-temporal atlas from infant brain images. Pairwise registrations are also only required between images of similar ages due to the limited support of the regression kernel.

References

1. Aljabar, P., Bhatia, K.K., Hajnal, J.V., Boardman, J.P., Srinivasan, L., Rutherford, M.A., Dyet, L.E., Edwards, A.D., Rueckert, D.: Analysis of growth in the developing brain using non-rigid registration. In: ISBI, pp. 201–204 (2006)
2. Arsigny, V., Commowick, O., Pennec, X., Ayache, N.: A log-euclidean framework for statistics on diffeomorphisms. In: Larsen, R., Nielsen, M., Sporring, J. (eds.) MICCAI 2006. LNCS, vol. 4190, pp. 924–931. Springer, Heidelberg (2006)
3. Avants, B.B., Epstein, C.L., Grossman, M., Gee, J.C.: Symmetric diffeomorphic image registration with cross-correlation: Evaluating automated labeling of elderly and neurodegenerative brain. Med. Image Anal. **12**(1), 26–41 (2008)
4. Bossa, M., Hernandez, M., Olmos, S.: Contributions to 3D diffeomorphic atlas estimation: application to brain images. In: Ayache, N., Ourselin, S., Maeder, A. (eds.) MICCAI 2007, Part I. LNCS, vol. 4791, pp. 667–674. Springer, Heidelberg (2007)
5. Cheng, S.H.U.N., Higham, N.J., Kenney, C.S., Laub, A.J.: Approximating the logarithm of a matrix to specified accuracy. SIAM J. Matrix Anal. Appl. **22**(4), 1112–1125 (1999)
6. Davis, B.C., Fletcher, P.T., Bullitt, E., Joshi, S.: Population shape regression from random design data. In: ICCV, pp. 1–7 (2007)
7. Habas, P.A., Kim, K., Corbett-Detig, J.M., Rousseau, F., Glenn, O.A., Barkovich, A.J., Studholme, C.: A spatiotemporal atlas of MR intensity, tissue probability and shape of the fetal brain with application to segmentation. NeuroImage **53**(2), 460–470 (2010)

8. Joshi, S., Davis, B., Jomier, M., Gerig, G.: Unbiased diffeomorphic atlas construction for computational anatomy. NeuroImage **23**(suppl. 1), S151–S160 (2004)
9. Kuklisova-Murgasova, M., Aljabar, P., Srinivasan, L., Counsell, S.J., Doria, V., Serag, A., Gousias, I.S., Boardman, J.P., Rutherford, M.A., Edwards, A.D., Hajnal, J.V., Rueckert, D.: A dynamic 4D probabilistic atlas of the developing brain. NeuroImage **54**(4), 2750–2763 (2011)
10. Ledig, C., Wright, R., Serag, A., Aljabar, P., Rueckert, D.: Neonatal brain segmentation using second order neighborhood information. In: Workshop on Perinatal and Paediatric Imaging: PaPI, MICCAI, pp. 33–40 (2012)
11. Lorenzi, M., Ayache, N., Frisoni, G.B., Pennec, X.: LCC-Demons: a robust and accurate symmetric diffeomorphic registration algorithm. NeuroImage **81**, 470–483 (2013)
12. Modat, M., Cardoso, M.J., Daga, P., Cash, D., Fox, N.C., Ourselin, S.: Inverse-consistent symmetric free form deformation. In: Dawant, B.M., Christensen, G.E., Fitzpatrick, J.M., Rueckert, D. (eds.) WBIR 2012. LNCS, vol. 7359, pp. 79–88. Springer, Heidelberg (2012)
13. Modat, M., Daga, P., Cardoso, M.J., Ourselin, S., Ridgway, G.R., Ashburner, J.: Parametric non-rigid registration using a stationary velocity field. In: MMBIA, pp. 145–150 (2012)
14. Modat, M., Ridgway, G.R., Taylor, Z.A., Hawkes, D.J., Fox, N.C., Ourselin, S.: A parallel-friendly normalised mutual information gradient for free-form registration. In: SPIE (2009)
15. Niethammer, M., Huang, Y., Vialard, F.-X.: Geodesic regression for image time-series. In: Fichtinger, G., Martel, A., Peters, T. (eds.) MICCAI 2011, Part II. LNCS, vol. 6892, pp. 655–662. Springer, Heidelberg (2011)
16. Pluim, J.P.W., Maintz, J.B.A., Viergever, M.A.: Mutual-information-based registration of medical images: a survey. IEEE TMI **22**(8), 986–1004 (2003)
17. Rueckert, D., Sonoda, L.I., Hayes, C., Hill, D.L., Leach, M.O., Hawkes, D.J.: Non-rigid registration using free-form deformations: application to breast MR images. IEEE Trans. Med. Imaging **18**(8), 712–721 (1999)
18. Serag, A., Aljabar, P., Ball, G., Counsell, S.J., Boardman, J.P., Rutherford, M.A., Edwards, A.D., Hajnal, J.V., Rueckert, D.: Construction of a consistent high-definition spatio-temporal atlas of the developing brain using adaptive kernel regression. NeuroImage **59**(3), 2255–2265 (2012)
19. Singh, N., Hinkle, J., Joshi, S., Fletcher, P.T.: A vector momenta formulation of diffeomorphisms for improved geodesic regression and atlas construction. In: ISBI, pp. 1219–1222 (2013)
20. Vercauteren, T., Pennec, X., Perchant, A., Ayache, N.: Symmetric log-domain diffeomorphic registration: a demons-based approach. In: Metaxas, D., Axel, L., Fichtinger, G., Székely, G. (eds.) MICCAI 2008, Part I. LNCS, vol. 5241, pp. 754–761. Springer, Heidelberg (2008)
21. Wright, R., Kyriakopoulou, V., Ledig, C., Rutherford, M.A., Hajnal, J.V., Rueckert, D., Aljabar, P.: Automatic quantification of normal cortical folding patterns from fetal brain MRI. NeuroImage **91**, 21–32 (2014)
22. Yushkevich, P.A., Avants, B.B., Das, S.R., Pluta, J., Altinay, M., Craige, C.: Bias in estimation of hippocampal atrophy using deformation-based morphometry arises from asymmetric global normalization: an illustration in ADNI 3T MRI data. NeuroImage **50**(2), 434–445 (2010)